Production of Extracellular Glycogen by Pseudomonas fluorescens: Spectroscopic Evidence and Conformational Analysis by Biomolecular Recognition

ARTICLE *in* BIOMACROMOLECULES · JUNE 2012

Impact Factor: 5.75 · DOI: 10.1021/bm300497c · Source: PubMed

4 AUTHORS, INCLUDING:

Fabienne Quilès
French National Centre for Scientific Research
38 PUBLICATIONS **564** CITATIONS
SEE PROFILE

Pavel Polyakov
Institut Pasteur International Network
21 PUBLICATIONS **260** CITATIONS
SEE PROFILE

Grégory Francius
French National Centre for Scientific Research
66 PUBLICATIONS **1,283** CITATIONS
SEE PROFILE

Article

pubs.acs.org/Biomac

Production of Extracellular Glycogen by *Pseudomonas fluorescens*: Spectroscopic Evidence and Conformational Analysis by Biomolecular Recognition

Fabienne Quilès,*[,†,‡] Pavel Polyakov,[†,‡,§] François Humbert,[†,‡] and Grégory Francius*[,†,‡]

[†]Université de Lorraine, Laboratoire de Chimie Physique et Microbiologie pour l'Environnement, LCPME, UMR 7564, Villers-lès-Nancy, F-54600, France

[‡]CNRS, Laboratoire de Chimie Physique et Microbiologie pour l'Environnement, LCPME, UMR 7564, Villers-lès-Nancy, F-54600, France

Supporting Information

ABSTRACT: Glycogen is mainly found as the principal storage form of glucose in cells. Many bacteria are able to synthesize large amounts of glycogen under unfavorable life conditions. By combining infrared spectroscopy, single molecule force spectroscopy (SMFS) and immuno-staining technique, we evidenced that planktonic *P. fluorescens* (Pf) cells are also able to produce glycogen as an extracellular polymeric substance. For this purpose, Pf suspensions were examined at 3 and 21 h of growth in nutritive medium (LB, 0.5 g/L). The conformation of the extracellular glycogen, revealed through its infrared spectral signature, has been investigated by SMFS measurements using Freely Jointed Chain model. The analysis of force versus distance curves showed over growth time that the increase of glycogen production was accompanied by an increase in glycogen contour lengths and ramifications. These results demonstrated that the production of extracellular bacterial glycogen can occur even if the cells are not subjected to unfavorable life conditions.

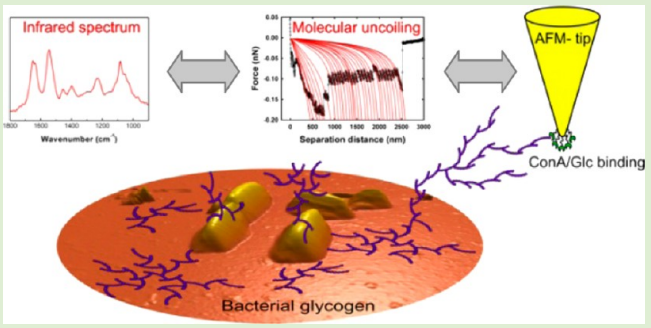

INTRODUCTION

In the last decades, numerous works have evidenced that bacteria have a great ability to synthesize a wide variety of polymers. Among these biomacromolecules, polyesters, glycoproteins, and oligopolysaccharides are increasingly studied because of the many fascinating potential applications in fields as diverse as plastics, pharmaceuticals, agro-alimentary, textile industry, or biomedicine.[1] These bacterial polymers either act as the part of energy reserves usually stored inside the cells or they are released outside the cells at their direct periphery; they are then called exopolymeric substances (EPS). The latter are often involved in adhesive properties and biofilm formation.[2] Polyhydroxyalkanoates (PHA), glycogen, and polyphosphate are known to be usually stored inside the microbial cells as a reserve of carbon, phosphate, and energy.[3] The production of PHA and glycogen occurs usually under conditions of limited growth and in the presence of an excess of carbon source.[3] *Pseudomonas* sp. are known for their ability to produce PHA.[3,4] One *Pseudomonas* sp. was found to synthesize both intracellular PHA and glycogen.[5] The production of intracellular glycogen was described in the literature for several bacteria but it is not usually the case for *Pseudomonas* sp.[3] For *Escherichia coli* and *Klebsiella pneumoniae* strains, it was suggested that the glycogen is in part linked to the peptidoglycan and localized in the periplasm.[6] For some gram positive bacteria, glycogen (or a "glycogen-like" glucan) was formed as an extracellular capsule.[7,8] Otherwise, EPS are produced and released in the external environment. For *P. fluorescens* (Pf) strains, exopolysaccharides are partly described as complex polymers containing several monomers of sugars.[9,10] EPS of some bacteria have also been tentatively characterized by infrared spectroscopy after their isolation and their purification.[11−13] However, the physicochemical characterization of EPS is complicated because it requires several steps of extraction and purification. Moreover, it always remains a doubt about what has been extracted. Mild extraction conditions fail to obtain the high molecular-weight fraction of EPS, whereas harsh extraction conditions are likely to rupture cell membranes, resulting in contaminating EPS extracts with intracellular compounds. Therefore, an in situ characterization, directly on live cells, would be preferable. Infrared spectroscopy is known to reach in situ the evolution of the whole chemical composition of bacteria at different growth phases and in different environments.[14−16] The specific staining of the bacteria also gives information on the chemical composition of the bacterial samples, as it was shown for the EPS of biofilms.[17−19] Atomic

Received: March 29, 2012
Revised: June 5, 2012

   dx.doi.org/10.1021/bm300497c | *Biomacromolecules* XXXX, XXX, XXX−XXX

force microscopy (AFM) emerged within the past decade into a powerful tool for various physical and biological applications.[20−23] It can operate under wet or physiological conditions[24,25] with a spatial resolution as high as ∼0.2 nm. AFM force spectroscopy now allows probing of the mechanical properties of soft biological samples[26,27] and the measurement of inter- and intramolecular interactions between the biomolecules.[28−30] Furthermore, physicochemical parameters such as the bacterial volumic charge density or the turgor pressure of bacteria covered by specific proteins, polysaccharides or lipopolysaccharides, are now accessible by AFM.[31] Combining the attenuated total reflectance Fourier transform infrared (ATR-FTIR) spectroscopy, the epifluorescence microscopy, and the AFM force spectroscopy, the production of glycogen by planktonic Pf is evidenced, and the investigation at the molecular scale of this is performed in this work. It includes the chemical identification, the conformational, and the adhesive properties. The results of this work establish for the first time the occurrence of extracellular glycogen for planktonic Pf.

EXPERIMENTAL SECTION

Chemicals. Glycogen from bovine liver (type IX, purity ≥ 85%), concanavalin A (Type IV), trishydroxymethylaminomethane (Tris), maleic acid, $MnCl_2$, and $CaCl_2$ were purchased from Sigma-Aldrich and used as received. Sybr Green II and Concanavalin A labeled with Texas Red (Molecular Probes) were purchased from Invitrogen. Tris-maleic buffer solution (pH∼5) for Concanavalin A was a mixture of Tris (0.06 M), maleic acid (0.04 M), $MnCl_2$ (0.001 M), and $CaCl_2$ (0.001 M).

Bacterial Strain and Culture Conditions. *Pseudomonas fluorescens* CIP 69.13 was purchased from the collection of the Pasteur Institute (Paris, France). It was cultured in Luria−Bertani broth (LB; Difco Laboratories) at 25 $g{\cdot}L^{-1}$, at 28 ± 1 °C, and under magnetic stirring as described elsewhere.[16] Briefly, the cells were incubated in order to reach the end of the exponential growth phase. The bacterial growth was monitored by measuring the optical density at 620 nm (OD_{620}) using a UNICAM Heλios ε visible spectrophotometer.

Planktonic *P. fluorescens* Suspensions for the Analyses. Bacteria at the end-exponential phase were harvested by centrifugation (8000 rpm, 10 min, 4 °C), and the pellet was resuspended in 200 mL of sterile LB medium (0.5 $g{\cdot}L^{-1}$). Bacterial concentration was adjusted to OD_{620} = 0.28 that corresponds to approximately 10^8 $CFU{\cdot}mL^{-1}$. This suspension, called S0, was cultured at 21 ± 1 °C under magnetic stirring (300 rpm). After 3 h, two new suspensions were prepared by dilution of 10 mL of S0 in 200 mL of fresh sterile LB medium (0.5 $g{\cdot}L^{-1}$). These new suspensions, called S1, were cultured for 3 h (S1−3h) and 21 h (S1−21h) at 21 ± 1 °C under magnetic stirring (300 rpm). To concentrate the bacterial suspensions for further analysis, suspensions S1−3h and S1−21h were then centrifuged (5000 rpm, 10 min, 4 °C), and the resulting pellets were resuspended in 4 and 10 mL, respectively, of media, as described in the following. For the recording of the AFM images, the pellets were resuspended in phosphate buffer saline solution (PBS) at pH ∼ 7.4. For the infrared analysis and the study of bacteria with Concanavalin A, the pellets were resuspended in Tris-maleic buffer at pH ∼ 5. The samples were then analyzed immediately.

Epifluorescence Optical Microscopy and Immunostaining. Samples were visualized by fluorescent staining using Sybr Green II and then lectin Concanavalin A−Texas Red (ConA-Tx). Sybr Green II (excitation wavelength at 480 ± 10 nm, observation emission wavelength at 520 nm) stains nucleic acids. ConA-Tx (excitation wavelength at 530 ± 20 nm, observation emission wavelength at 590 nm) stains specifically α-glucosyl and α-mannosyl residues.[32,33] A total of 2 mL of final suspensions S1−3 h or S1−21 h were mixed with 1 μL of the commercial Sybr Green II solution (Molecular Probes from Invitrogen) and laid on a germanium disk for 20 min in the dark at 21 ± 1 °C. The Ge disk was then rinsed with nonpyrogenic sterile water to eliminate excess Sybr Green II and wicked dry with filter paper to remove excess water. Then, the bacteria on the Ge disk were stained with 0.5 mL of a solution of ConA-Tx (0.5 g/L in Tris-maleic buffer, beforehand centrifuged at 9000 rpm during 10 min to remove aggregates) for 20 min in the dark. The Ge disk was then rinsed with nonpyrogenic sterile water to eliminate excess ConA-Tx, and wicked dry with filter paper to remove excess water. The samples were visualized with an Olympus BX51 microscope using immersion oil 100× objective and equipped with an Olympus XC50 camera. Two separate pictures were recorded at the same place to visualize the fluorescence of both dyes.

ATR-FTIR Spectroscopy. ATR-FTIR spectra were recorded between 4000 and 800 cm^{-1} on a Bruker Vector 22 spectrometer equipped with a KBr beam splitter and a DTGS detector and driven by the OPUS 3.1 software. The resolution of the single beam spectra was 4 cm^{-1}. A nine-reflection diamond ATR accessory (Durasampl*IR*, SensIR Technologies, incidence angle: 45°) was used for acquiring spectra. The number of bidirectional double-sided interferogram scans was 100, which corresponds to a 1 min accumulation. All interferograms were Fourier processed using the Mertz phase correction mode and a Blackman-Harris three-term apodization function.[34] No ATR correction was performed. Measurements were performed at 21 ± 1 °C in an air-conditioned room. One drop of the bacterial suspensions in Tris-maleic buffer or glycogen solution in water was put on the ATR crystal. Appropriate spectra were used to remove the spectral background: a Tris-maleic buffer spectrum for the bacterial suspensions and a water spectrum for the glycogen solution. Water vapor subtraction was performed when necessary.

AFM Measurements. AFM images and force−distance curves were recorded using an MFP3D-BIO instrument (Asylum Research Technology, Atomic Force F&E GmbH, Mannheim, Germany). Silicon nitride cantilevers of conical shape were purchased from Atomic Force (OMCL-TR400PSA-3, Olympus, Japan) and their spring constants were determined using the thermal calibration method,[35] providing values of about 20−25 pN/nm. Prior to each experiment, the geometry of the tip was systematically controlled using a commercial grid for 3D visualization (TGT1, NT-MTD Company, Moscow, Russia), and the curvature of the tip at its extremity was found to lie in the range of 15−30 nm. Cells were electrostatically immobilized onto polyethyleneimine (PEI)-coated glass slides.[36] Such a method avoids the necessity to resort to chemical binders between the substrate and the bacterial sample, thus, minimizing any chemical modification of the bacterial cell wall/surface organization. Glass slides were freshly prepared upon immersion in 0.2% PEI solution for 30 min, extensively rinsed with Milli-Q water, then dried with nitrogen and stored in a sterile Petri dish. A total of 1 mL of bacterial suspension was directly deposited onto the PEI-coated glass slide for 20 min, and then the bacteria-coated surface was extensively rinsed 3 times with Milli-Q water. Following this step, the sample was immediately transferred into the AFM liquid cell with addition of 2 mL of PBS solution at pH ∼ 7.4 for the imaging and the nanomechanical analysis. For the recording of images in air using the contact mode (applied force below 250 pN), the bacteria-coated PEI surfaces were rinsed and gently dried with nitrogen. Single molecule force experiments were performed with 2 mL of Tris-maleic buffer solution and AFM tips were functionalized with Concanavalin A (ConA, Sigma-Aldrich,). This functionalization was performed via a 6 nm-long polyethylene glycol (PEG) chain using a protocol previously described (Figure S1 in Supporting Information):[21,37] Cantilevers were washed with chloroform and ethanol, placed in an UV-ozone-cleaner for 30 min, and incubated overnight in a solution of ethanolamine hydrochloride in DMSO (3.3 g in 6 mL) to generate amino groups on the tip surface.[38] These amino groups reacted with PEG linkers carrying benzaldehyde functions on their free-tangling end, essentially as described elsewhere.[39] For the coupling of the lectins, the cantilever was covered with a 200 μL droplet of a PBS solution containing ConA (0.1 g/L) to which 2 μL of a 1 M $NaCNBH_3$ solution was added. After 50 min of incubation, 5 μL of a 1 M ethanolamine hydrochloride solution (pH 9.5) was added to deactivate the nonreacted aldehyde

dx.doi.org/10.1021/bm300497c | *Biomacromolecules* XXXX, XXX, XXX−XXX

groups during another 10 min incubation period, after which the cantilever was washed with and stored in PBS.

Single Molecule Force Spectroscopy and Force Volume Images Data Processing. Nanomechanical properties and conformational characteristics of biomacromolecules were measured by recording Force-Volume Images (FVI) consisting of a grid of 32-by-32 and 16-by-16 force curves obtained upon approach and subsequently retraction of the tip (single molecule force spectroscopy for SMFS experiments). Bacterial Young modulus E was obtained by interpreting the force curves versus the indentation curves according to the Sneddon model.[40,41] In this model, loading force F is given by

$$F = \frac{2E \tan \sigma}{\pi(1-\nu^2)}\delta^2 \quad (1)$$

where δ is the indentation depth, ν is the Poisson coefficient, and σ is the semitop angle of the tip. Equation 1 refers to our cases where the compression and the deformation of a soft planar interface are occasioned by a tip of conical geometry. The turgor pressure is the inner osmotic pressure in the cytoplasm that maintains the bacterial shape.[42] It was calculated from the linear regime of the indentation. The turgor pressure estimations were performed from bacterial spring constant k_{cell} according to the equation

$$k_{cell} = \frac{3}{2}\pi p a \frac{K_1(\rho^*)}{K_0(\rho^*)} \quad (2)$$

where p is the turgor pressure, a is the bacterium radius (~400 nm), K_0 and K_1 are modified Bessel functions of the second type of order 0 and 1, respectively, and ρ^* stands for the reduced curvature radius defined by

$$\rho^* = \rho\left[\frac{3pR^3}{4(\lambda - pR)}\right]^{-1/2} \quad (3)$$

where ρ is the cantilever tip radius ($\rho \sim 20$ nm) and λ is the stretching modulus of the bacterial envelope ($0.1 \leq \lambda \leq 0.2$ N/m). Bacterial spring constant k_{cell} was calculated from the force versus indentation curves in the linear regime, that is, for a loading force higher than 2 nN. This parameter corresponds to the slope of the force versus indentation curve, as shown in Supporting Information (Figure S2).

For each sample, the nanomechanical analysis was performed on six bacterial cells by recording two FVI of 20 or 10 μm sizes and six FVI of 500 nm size taken over different bacterial cell walls.

In SMFS experiments, the biomacromolecules located on the surface or around the biological sample are stretched upon removal of the chemically modified AFM tip away from the surface. The obtained force curves versus the distance curves are then analyzed with the FJC (Free Jointed Chain) model.[43−45] This model is the most suitable and the most frequently used to describe the extension of polysaccharides.[21,37,45−47] Extension z_{FJC} of the macromolecule is related to retraction force F_{adh} via eq 2:[43,44]

$$z_{FJC} = -L_c\left[\coth\left(\frac{F_{adh}L_k}{k_bT}\right) - \frac{k_bT}{FL_k}\right] \quad (4)$$

where Kuhn length L_k is a direct measure of the chain stiffness, L_c is the total contour length of the macromolecule, and k_b is the Boltzmann constant.

The number of monomers in the polysaccharidic chains was deduced from eq 4 by replacing L_c by $N{\cdot}L_k$ (N is an integer) following eq 5:

$$z_{FJC} = -N{\cdot}L_k\left[\coth\left(\frac{F_{adh}L_k}{k_bT}\right) - \frac{k_bT}{FL_k}\right] \quad (5)$$

All the FVI were analyzed with an automatic Matlab algorithm described elsewhere[31] for appropriate theoretical models (Figure S3 in Supporting Information). For each sample, two FVI of 20 × 20 μm size and five FVI of 5 × 5 μm size taken over different bacterial cells were recorded. Note that force curves were performed on freshly PEI-coated glass slice and glucose-grafted gold surface to verify the binding specificity of the AFM tip (Figures S1 and S4 in Supporting Information).

RESULTS AND DISCUSSION

ATR-FTIR Identification of Glycogen from Planktonic *P. fluorescens* Suspensions. Figure 1 shows the ATR-FTIR

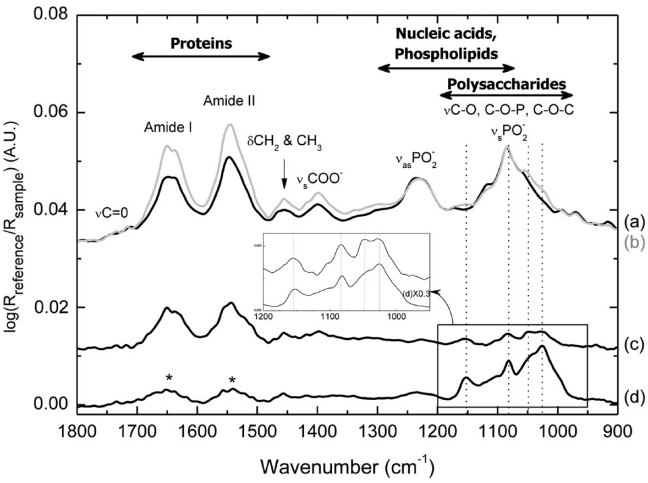

Figure 1. ATR-FTIR spectra of (a) and (b) *P. fluorescens* planktonic bacteria in Tris-maleic buffer from S1−3h (in black) and S1−21h (in gray) suspensions, respectively; (c) = (b) − (a); (d) commercial glycogen at 5 g/L in water (*protein impurities in the commercial product). Spectra (a) and (b) are normalized with respect to the band near 1080 cm^{-1}. The inset shows an expended region 1200−900 cm^{-1} for spectra (c) and (d). Offsets of spectra are used for clarity.

spectra for bacterial suspensions S1 grown in LB medium at 0.5 g·L^{-1} during 3 h (Figure 1a) and 21 h (Figure 1b). The general features of the spectra are similar and are characteristic of Pf.[16] The spectral region between 1800 and 1200 cm^{-1} shows clearly the occurrence of proteins, through Amide I and II bands, and phospholipids and nucleic acids through the phosphate asymmetric stretching band near 1230 cm^{-1}. Spectra (a) and (b) are normalized with respect to the band near 1080 cm^{-1}. Two major differences can be noted. First, the ratio {proteins}-to-{nucleic acids + phospholipids} is lower for bacteria from suspension S1−3h (Figure 1, curve a) with respect to bacteria from suspension S1−21h (Figure 1, curve b). The older bacteria probably synthesize less nucleic acids with respect to proteins after 21 h of culture because they should reach a stationary phase of growth. Second, the shape of the bands between 1200 and 1000 cm^{-1} changes. Difference spectrum (c) = (a) − (b) (Figure 1c and inset) clearly exhibited several bands at 1151, 1082, 1049, and 1026 cm^{-1} characteristic of the infrared fingerprint of glycogen. This finding suggests an overproduction of glycogen in bacterial suspension S1−21h. We have already observed by ATR-FTIR spectroscopy that a glycogen production could also take place under some conditions over the initial stages of the Pf biofilm formation.[48] The slight differences in the relative intensities, in particular, in the 900−1300 cm^{-1} region, between spectra (c) and (d) may result from the quality of commercial glycogen (purity ≥ 85%) and other changes in the biochemical composition of bacteria in suspension S1−21h with respect to those in suspension S1−3h, as exemplified in the ratio {proteins}-to-{nucleic acids + polysaccharides + phospholipids}. From these results, we can suggest that the glycogen production by Pf occurs under these

dx.doi.org/10.1021/bm300497c | *Biomacromolecules* XXXX, XXX, XXX−XXX

conditions of growth, while the production of glycogen was not observed in the spectra of Pf cultured in other LB medium conditions.[16] Glycogen is usually accumulated inside the bacterial cells and it is considered to function as an energy reserve for many bacteria[3] but rarely[5] for *Pseudomonas* sp. that have frequently been reported to rather produce PHA.[3,4] The infrared signature of PHA[49] was not detected in the present work. Several works found that EPS from Pf were a mixture of several sugars such as mannose, glucose and galactose[9,10,50,51] but not precisely glycogen. Mannan and galactan were not detected in the IR-ATR spectra obtained in this work (see Bahmed et al.[52] and Figure S5 in Supporting Information, respectively). At this stage, it is unknown whether the glycogen detected here is contained within the cells or is a component of the EPS, as ATR-FTIR spectroscopy only yields an average chemical composition of the whole sample.

Evidence of Extracellular Polysaccharides of Planktonic *P. fluorescens* by Epifluorescence Microscopy. Figure 2 shows the epifluorescence images of bacteria from

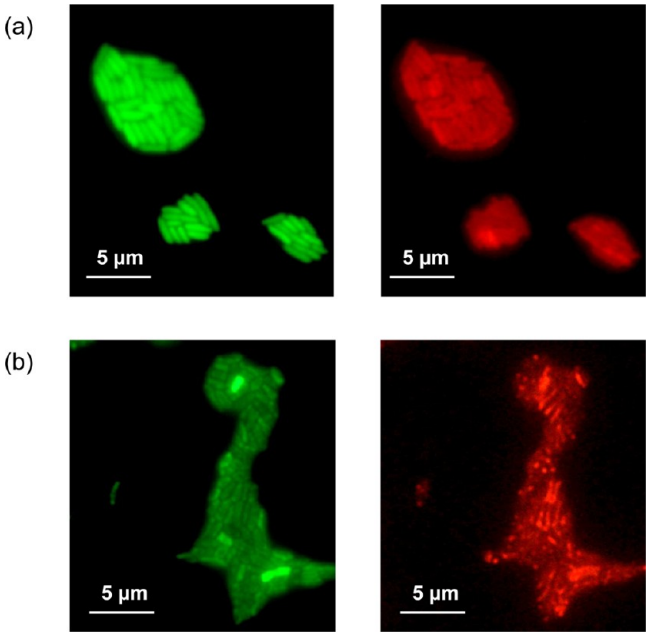

Figure 2. Epifluorescence microscopy images of bacterial suspensions of *P. fluorescens* droplets on a Ge crystal. (a) Bacteria from S1−3h suspension; (b) bacteria from S1−21h suspension. Bacteria were stained with Sybr Green II (left images), and then with Concanavalin A−Texas Red (right images).

suspensions S1−3h and S1−21h stained with Sybr Green II that is specific to nucleic acids, it penetrates the cells, and with ConA-Tx that is specific to the glucosyl and mannosyl residues. ConA does not penetrate the cells, and it was used as a probe to examine the EPS.[17] The average sizes of the bacteria were 2.0 × 0.6 and 1.5 × 0.6 μm for cells from S1−3h and S1−21h suspensions, respectively. These results are discussed in the next section. Sybr Green II fluorescence was more intense and more evenly distributed in the cells from suspension S1−3h than in the cells from suspension S1−21h (Figure 2). Figure 2a (right) shows that bacterial cells are covered with ConA-reactive extracellular polysaccharides, and the fluorescence of ConA-Tx was localized precisely on all the bacterial surfaces. In contrast, the epifluorescence images of bacteria from S1−21h show discontinuous red fluorescent regions rather localized on the periphery of the bacteria (Figure 2b, right). The differences observed for the green fluorescence may be due to the occurrence of a high amount of EPS around the bacteria that partly prevents or slows down the Sybr Green II penetration. Given the binding specificities of ConA-Tx for α-glucosyl and α-mannosyl residues, the images suggest that planktonic Pf releases over time, and under this culture condition, EPS containing glucose and/or mannose. Because the ATR-FTATR spectra did not exhibit the vibrational signature of mannan,[52] EPS contained very little or no mannose.

Morphological and Nanomechanical Properties of Planktonic *P. fluorescens*. Figure 3 shows AFM images of Pf

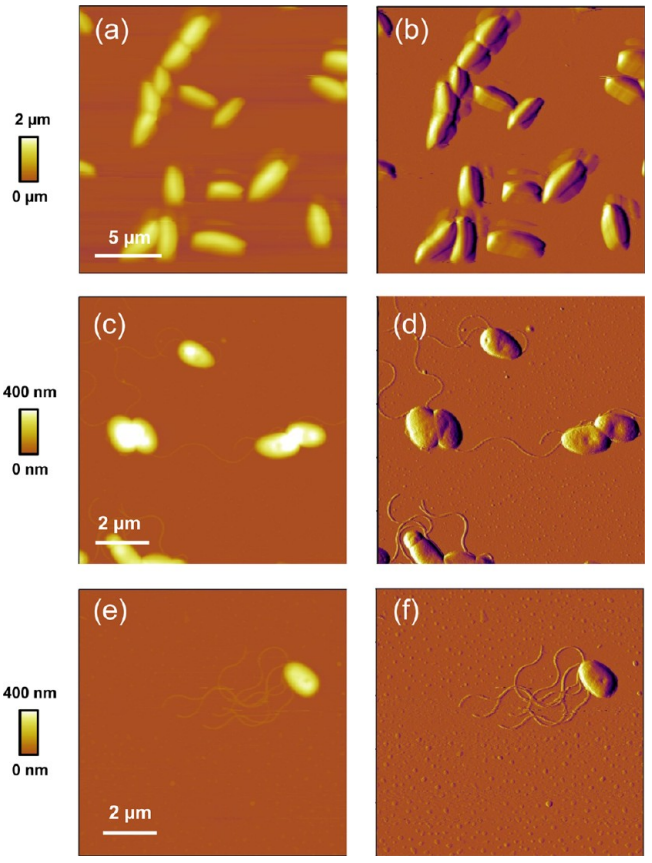

Figure 3. AFM imaging of *P. fluorescens* cells: (a) and (b) height and deflection images in PBS buffer solution of live cells from S1−3h suspension, respectively; (c) and (d) height and deflection images in air of dehydrated cells from S1−3h suspension, respectively; (e) and (f) height and deflection images in air of dehydrated cells from S1−21h suspension, respectively.

immobilized onto PEI-coated glass surfaces. As previously observed for AFM imaging of bacteria,[21] the resolution of the height images of Pf in their native state (Figure 3a,b) was limited by the large curvature of the rod-shaped cells while deflection images were more sensitive to the surface relief. These AFM images showed a smooth morphology with size varying from 1 to 2 μm long for 0.5 to 0.7 μm diameter (Figure 8a,c, as shown in the next section), in accordance with epifluorescence measurements. Without saying that the bacteria were grown under nutrient stress, the lower nutrient charge, however, induces a low decrease in the length of the bacteria in LB 0.5 g/L with respect to LB at 25 g/L and also over culture time (between S1−3h and S1−21h), as shown by fluorescence

dx.doi.org/10.1021/bm300497c | *Biomacromolecules* XXXX, XXX, XXX−XXX

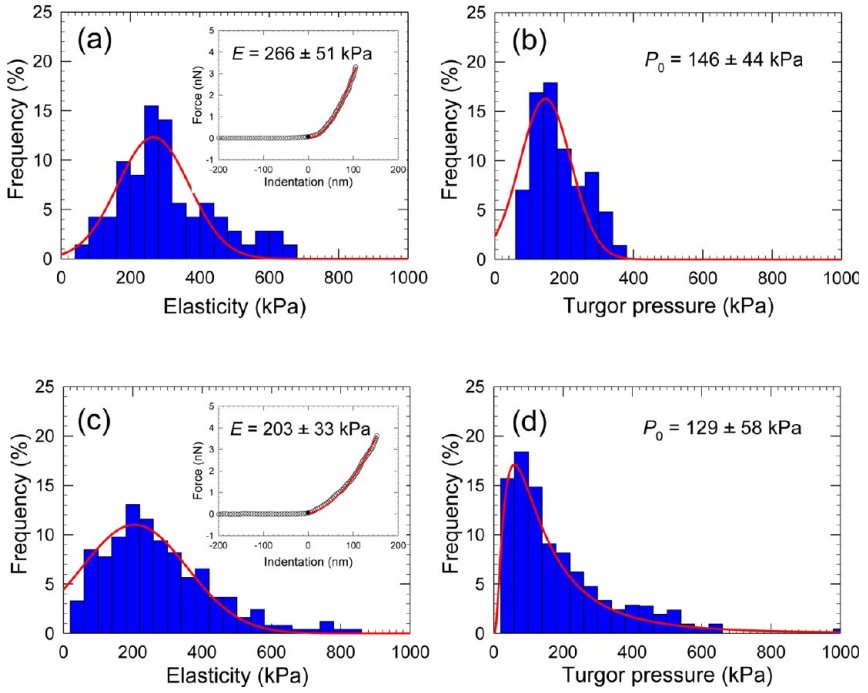

Figure 4. Nanomechanical properties for *P. fluorescens* cells in PBS solution. (a, c) Statistical distributions of bacterial cell wall elasticity from S1−3h and S1−21h suspensions, respectively. (b, d) Statistical distribution of bacterial turgor pressure from S1−3h and S1−21h suspensions, respectively. Insets: representative force−indentation curves with the theoretical model.

images. This phenomenon was already observed for some bacteria.[53] In contrast to the deflection images performed in aqueous medium, the images taken in air (Figure 3d,f) were significantly more sensitive to the bacterial surface relief and the morphological details. In addition, the images showed 1−6 flagella on one cell with 1−8 μm long for about 20 nm diameter (Figure 3f). These appendages seem to be fixed only at one pole of the bacterial cells. These observations indicated at moderately rich nutrient conditions, Pf continues to produce flagella. Besides, no polymeric structures as EPS could be detected over the cell walls or surrounding the cells, in contrast to what was observed on diatoms or lactic bacteria.[21,26] The absence of such structures on the AFM contact mode image could be due to the AFM resolution limit. The nanomechanical properties of the bacterial cells from S1−3h and S1−21h suspensions were determined using the nanoindentation technique. The AFM force−distance curves were recorded and subsequently analyzed according to previous works.[31] The statistical distributions of the bacterial cell wall elasticity (Figure 4a,c), and the inner turgor pressure (Figure 4b,d) for bacteria from S1−3h and S1−21h were measured. Both the cell wall elasticity and the turgor pressure decreased with the increase in the culture time. They varied from 266 and 146 kPa to 203 and 129 kPa, respectively. The decrease in the elasticity could probably be attributed to the occurrence of EPS that modifies the cell wall elasticity.[21]

Single Molecule Force Analysis of *P. fluorescens* Extracellular Polymers. Single-molecule force spectroscopy (SMFS) is a more sensitive technique than AFM imaging, and it would be more efficient to detect the presence of EPS on the bacteria.[37] The retraction force curves recorded on the bacterial suspensions using ConA functionalized AFM-tips were specific to α-glucose and α-mannose residues. Figure 5 shows two retraction force curves taken on bacteria from suspensions S1−3h and S1−21h. Molecular elongations up to 800 nm (Figure 5a) and up to 2500 nm (Figure 5b) were recorded for bacteria from suspensions S1−3h and S1−21h, respectively. This result highlights that extracellular polymers detected here, are rich in

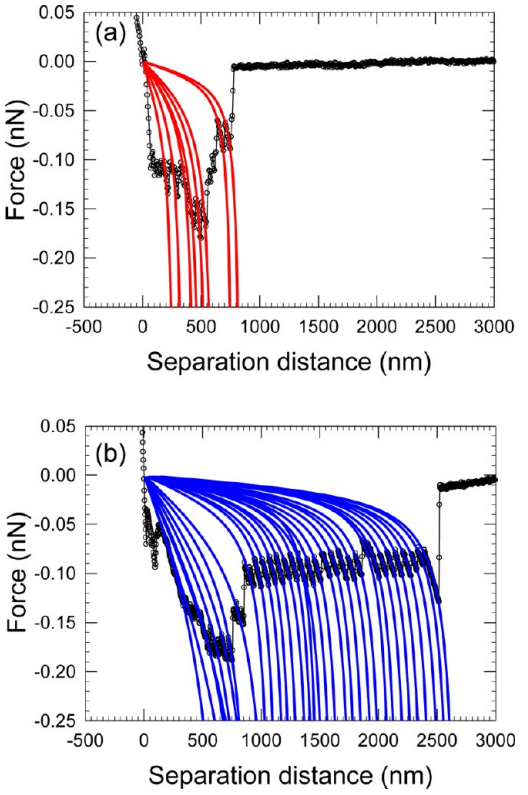

Figure 5. Examples of retraction force curves performed by SMFS (empty circles) on *P. fluorescens* cells immobilized in PEI-coated glass and corresponding FJC fittings (red and blue lines). (a) Bacterial cells from S1−3h suspension; (b) bacterial cells from S1−21h suspension.

dx.doi.org/10.1021/bm300497c | *Biomacromolecules* XXXX, XXX, XXX−XXX

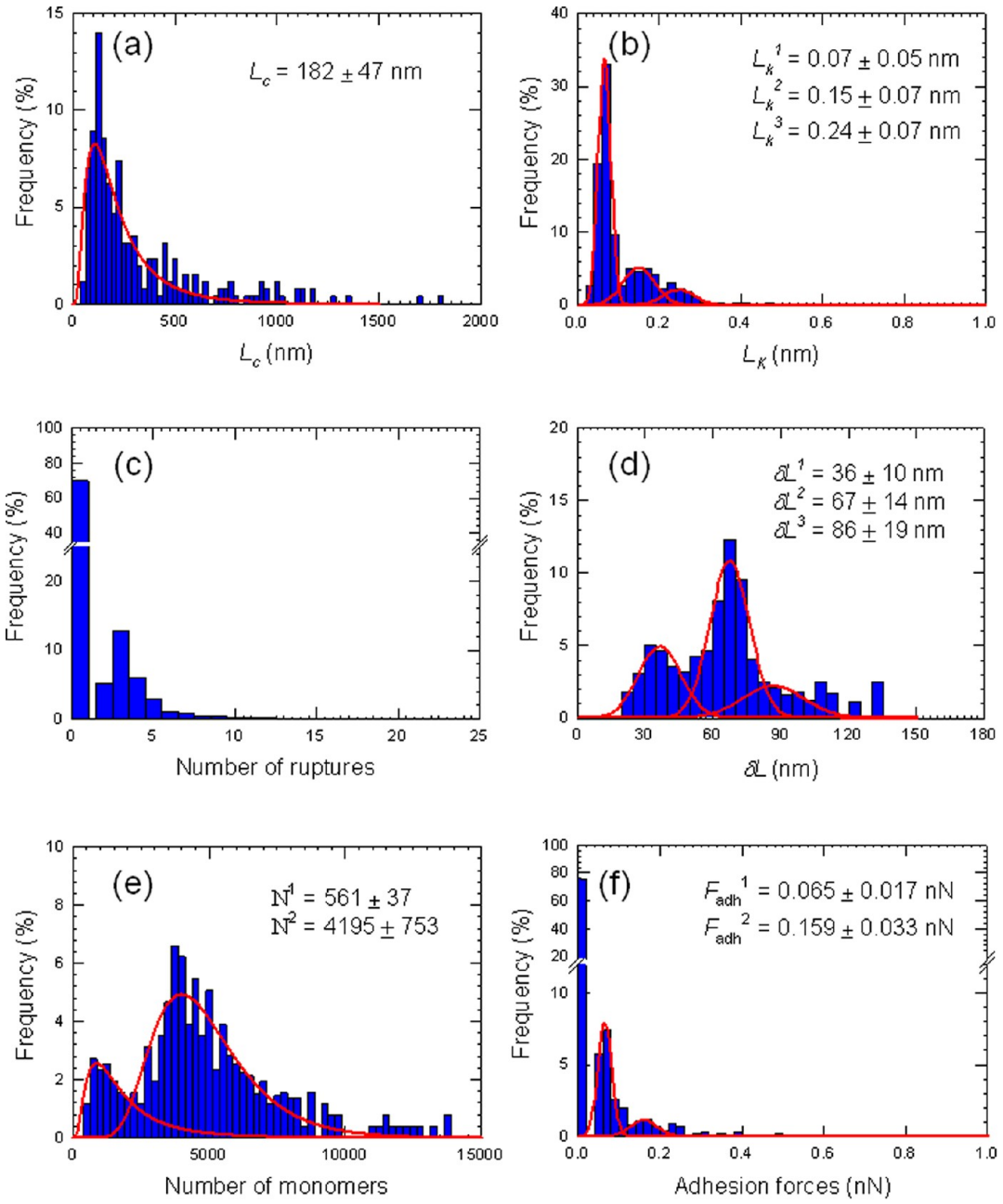

Figure 6. Physico-chemical properties of *P. fluorescens* exopolymers from S1−3h suspension: (a) statistical distribution of the contour length; (b) statistical distribution of the Kuhn length; (c) statistical distribution of the number of ruptures; (d) statistical distribution of the distance between two consecutive adhesion force ruptures; (e) statistical distribution of the number of monomers constituting the polysaccharidic chains; (f) statistical distribution of the adhesion force (amplitude of the last adhesive event).

α-glucose and α-mannose. The ATR-FTIR spectra identified glycogen, that is, bacterial exopolymers contained α-glucose. In fact, the features of both force curves were generally similar below 800 nm, and above this value, curves recorded on the bacteria from the S1−21h suspension showed additional very regular adhesion peaks (Figure 5b).

The full analysis of all the Force Volume Images (FVI) recorded with the Freely Jointed Chain (FJC) model should enable us to better understand the possible molecular changes that occurred on bacteria at two times of culture in LB 0.5 g/L. The FJC model fitted with good agreement the experimental curves. The fittings were significantly different for both types of curves. Six parameters taken from the FVI analysis were examined: contour length L_c, Kuhn length L_k, number of monomers N, distance δL between two consecutive adhesive events, the number of adhesion peaks (i.e., the number of ruptures in the retraction force curves), and the last adhesion forces which is characteristic to the last adhesive event. Figures 6 and 7 report the statistical distributions of the parameters calculated from the whole force curves for the bacterial cells from suspensions S1−3h and S1−21h, respectively.

The total contour lengths of the macromolecules at the bacterial surface show a wide range from 200 to 2000 nm, with most frequent values of $L_c \approx 182$ nm (Figure 6a) and 502 nm (Figure 7a). The macromolecules detected on the bacteria from S1−21h were much longer than those detected on bacteria

dx.doi.org/10.1021/bm300497c | *Biomacromolecules* XXXX, XXX, XXX−XXX

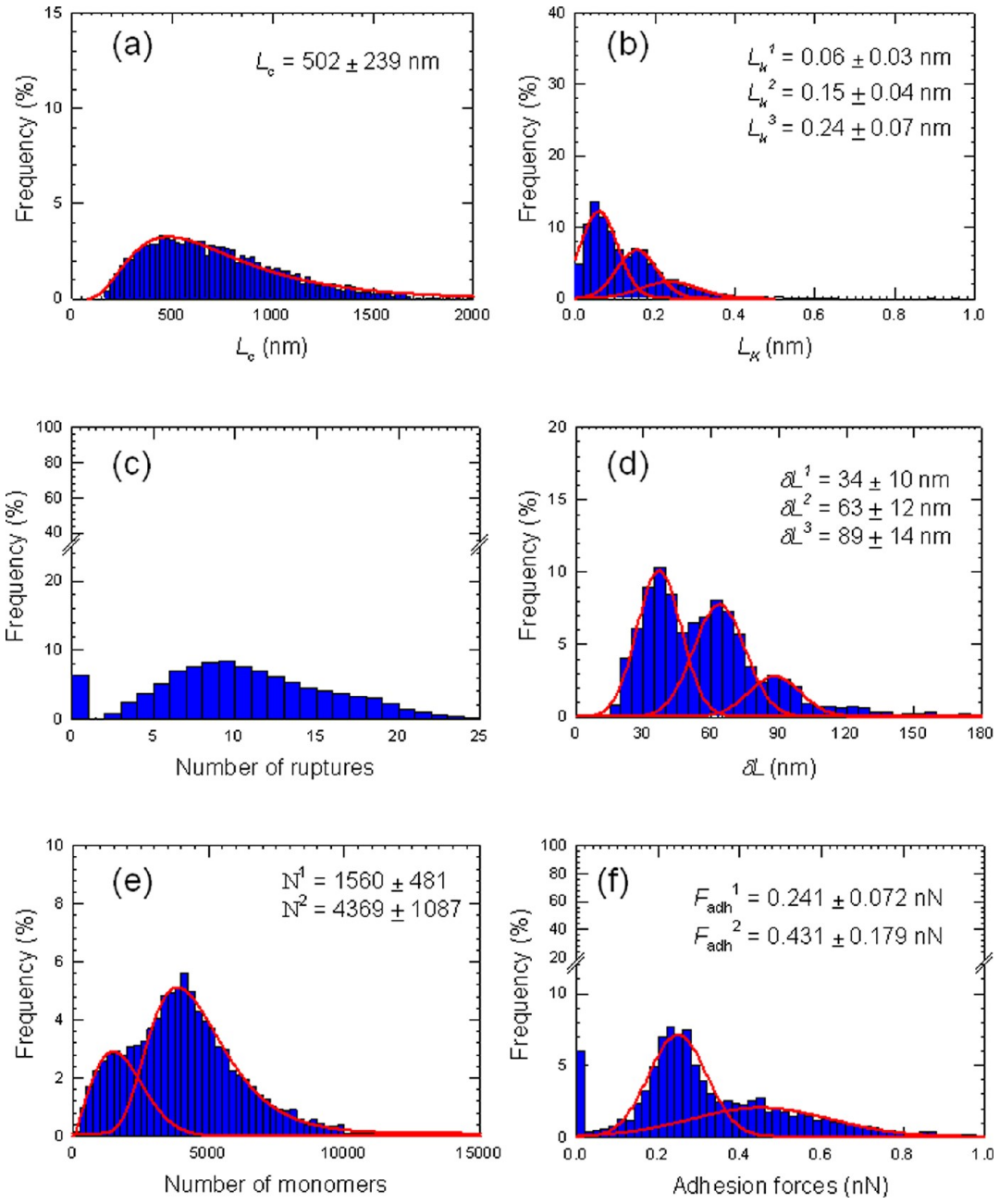

Figure 7. Physico-chemical properties of *P. fluorescens* exopolymers from S1−21h suspension: (a) statistical distribution of the contour length; (b) statistical distribution of the Kuhn length; (c) statistical distribution of the number of ruptures; (d) statistical distribution of the distance between two consecutive adhesion force ruptures; (e) statistical distribution of the number of monomers constituting the polysaccharidic chains; (f) statistical distribution of the adhesion force (amplitude of the last adhesive event).

from S1−3h (see also Figure 5). A molecular growth can be suggested as a function of the culture time.

The statistical distribution of L_k shows three maxima at $L_k \sim$ 0.07, 0.15, and 0.24 nm (Figures 6b and 7b). These values were very similar for both samples. The first value corresponds to the elongation of a single sugar molecule following a conformational change of a C_5-C_6 bond position, the second value corresponds to the length of a C−C bond, and the third value can be attributed to the length of one sugar monomer.[21,46] Indeed, in previous works a Kuhn length of about 1.2 to 1.4 nm was calculated for *Lactobacillus rhamnosus* EPS,[21] which consists of a repetition of six sugars.[54,55]

Figure 6c shows that 1−10 uncoiling/rupture events can be detected over the whole retraction curves forming the FVI. From Figure 7c, 1−25 uncoiling/rupture events were detected. These results suggested that Pf EPSs were bonded at several points over the AFM-tip, EPS should therefore be ramified.

Parameter δL is related to the length between two successive ruptures in the polymer chain. The statistical distributions in δL (Figures 6d and 7d) show three close maxima near 30, 60, and 90 nm for both samples. However, the frequency distribution changes between both samples. A maximum is observed at 60 nm for S1−3 h suspension. A continuous decrease of the δL distribution can be observed from 30 to 90 nm for bacteria from S1−21h, probably showing a more regular structure. The

dx.doi.org/10.1021/bm300497c | *Biomacromolecules* XXXX, XXX, XXX−XXX

observed periodical length l_p of ~30 nm can be attributed to the shortest distance between two branches within a given glycogen chain. Indeed, previous works have evidenced that ConA binds the terminal sugar groups and not individual residues along a main chain.[33] Moreover, the good regularity between the ruptures (about 10−15 ruptures per curve) with a periodic length of about 30 nm indicated that several terminal glucosyl residues were detected, strongly suggesting a branched structure. Meléndez et al.[56] optimized several structural parameters of glycogen to achieve efficient fuel molecules for energy storage in cells (optimization of the cell metabolism). Their results showed that this molecule is formed by concentric glycogen fractal chains with 12 branches (Figure S3 in Supporting Information). A rough estimation from our data suggests 6−17 branches (L_c/l_p).

In addition, the statistical distributions (Figures 6e and 7e) which depict the distribution of the number of monomers, exhibit two distributions. Concerning EPS of bacteria from S1−3h, the first one accounts for about 15% of the polysaccharidic chains with 561 monomers, while the second one corresponds to about 85% of the polysaccharidic chains with 4195 monomers (Figure 6e). For EPS of bacteria from S1−21h, the first one accounts for about 38% of the polysaccharidic chains with 1560 monomers while the second one corresponds to about 62% of the polysaccharidic chains with 4369 monomers (Figure 7e). This result suggested the occurrence of both short and very long polysaccharidic chains (Figure 7d). Moreover, an increase of the ramifications is observed for the EPS of suspension bacteria from S1−21h.

The statistical distributions of adhesion forces (Figure 6f) evidenced that polysaccharides are absent or not detectable from about 80% of the total FVI area in the case of the bacterial sample from S1−3h. Only 7% of nonadhesive events were detected for the sample from S1−21h (Figure 7f), suggesting a higher production of EPS that are released in the medium.

The last rupture during the AFM-tip retraction corresponds to the physical detachment of the last glucose monomer of the macromolecule. The calibration experiment performed on model surface (Figure S4 in Supporting Information and literature[37]) showed that the detachment of one glucose molecule corresponds to about 60 pN. The amplitude of the last adhesion force is proportional to the number of macromolecules simultaneously detached from the AFM-tip for each force curve on average. For both bacterial samples, the adhesion forces extracted from the retraction curves were in the range of 0.05−0.40 nN. They were attributed to the simultaneous detection of 1−3 and 4−8 macromolecules in average per force−distance curve for S1−3h and S1−21h, respectively.

Spatially resolved force mappings allowed the localization of adhesive zones over the sample surface; that is, where EPS macromolecules were located. Figure 8a,c shows the reconstructed height images calculated from the FVI. The corresponding 2D force maps are presented in Figure 8b,d, and bacterial cells are indicated by the blue zones and EPS by the red ones. When comparing Figure 8b and d, it turns out that little polysaccharides cover the bacterial cells from suspension S1−3h, they were rather located next to the bacteria. For Pf from S1−21h, an increase in the sample coverage by macromolecules can be observed. In addition, the macromolecules were also mainly detected at the periphery of the bacteria. This observation confirms that the detected biopolymers were synthesized and excreted by the bacteria.

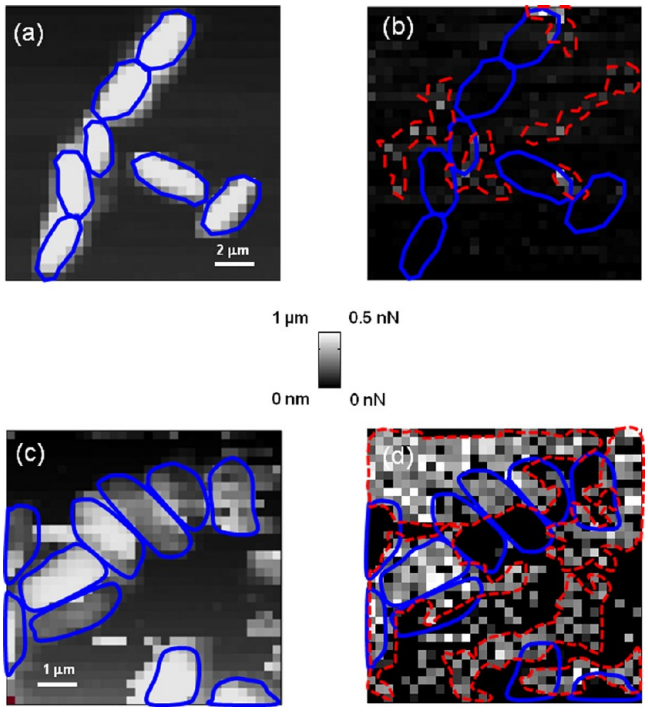

Figure 8. Maps of adhesive properties of *P. fluorescens*, and glycogen localization: (a) Deflection image of bacteria from S1−3h suspension; (b) adhesion force map (F-range = 0−0.5 nN) for the last adhesion force rupture measured on bacteria located on the surface as indicated in panel a; (c) deflection image of bacteria from S1−21h suspension; (d) adhesion force map (F-range = 0−0.5 nN) for the last adhesion force rupture measured on bacteria located on the surface as indicated in panel c. The blue zones correspond to bacterial cells location and the red zones to glycogen one.

These data are in accordance with immuno-staining measurements.

CONCLUSIONS

In this work, we have shown that *P. fluorescens* synthesizes extracellular glycogen, as an EPS, under moderately rich medium conditions. This demonstration was performed in situ on living bacteria. Evidence of the biosynthesis and the release of glycogen by planktonic *P. fluorescens* were shown thanks to the combination of ATR-FTIR, epifluorescence microscopy after immuno-staining, and AFM force spectroscopy. An increasing production of extracellular glycogen was observed with time under moderately rich culture conditions (LB 0.5 g/L). The average glycogen contour lengths and ramifications are increased by a factor of 3 and 2, respectively. Despite an increase of glycogen size, it keeps the same features for the Kuhn length's and for the number of monomers. Besides, parameter δL, that is, the distance between two consecutive adhesive events, only changes in terms of statistical distribution and not in absolute values. These observations suggested that the glycogen ramifications get closer between 6 and 24 h of total culture. Finally, it is surprising that these macromolecules, whose main function is usually bacterial energy storage, are released outside the cells, and not accumulated. The role of this peculiar biosynthesis is not known at this time. To the best of our knowledge, this is the first evidence and the first direct proof of production, release and structure determination of extracellular glycogen from planktonic *P. fluorescens* cells.

dx.doi.org/10.1021/bm300497c | *Biomacromolecules* XXXX, XXX, XXX−XXX

■ ASSOCIATED CONTENT

Supporting Information

Scheme of the chemical functionalization of the silicon nitride AFM-tip (Figure S1). Force curve modelings of the Young modulus and bacterial spring constant (a) and theoretical estimation of the turgor pressure (b; Figure S2). Schematic representation of FJC model and fractal structure of the glycogen (Figure S3). Statistical distribution of adhesion forces for ConA-tip during specificity control with representative force curves in the insets (Figure S4). ATR-FTIR spectrum of an aqueous solution of commercial galactan (Figure S5). Statistical distribution of adhesion forces for ConA-tip on PEI-coated glass surface with representative force curves in the insets (Figure S6). Typical elasticity map and representative force−indentation curves of bacteria from S1−3h (a) and S1−21h (b; Figure S7). Tables of mechanical properties corresponding to Figure S7 (Figure S7 cont.). Examples of retraction force curves performed by SMFS (empty circles) on *P. fluorescens* cells immobilized in PEI coated glass, and corresponding FJC (blue lines) and WLC (red lines) fittings (Figures S8−S10 cont.). This material is available free of charge via the Internet at http://pubs.acs.org.

■ AUTHOR INFORMATION

Corresponding Author

*E-mail: fabienne.quiles@lcpme.cnrs-nancy.fr (F.Q.); gregory.francius@lcpme.cnrs-nancy.fr (G.F.). Phone: (33) 03 83 68 52 34 (F.Q.); (33) 03 83 68 52 36 (G.F.).

Present Address

[§]Laboratoire Environnement et Minéralurgie, Université de Lorraine, and Laboratoire Environnement et Minéralurgie, CNRS, LEM, UMR 7569, Vandoeuvre-lès-Nancy, F-54501, France.

Notes

The authors declare no competing financial interest.

■ ACKNOWLEDGMENTS

G.F. and P.P. gratefully thank Pr. D. Brie and Dr. C. Soussen for assistance in the SMFS data processing. The authors thank Dr. A. Zegeye for rereading of the text. This work was financially supported by the French Program ANR-07-JCJC-0024-01 PHYSCHEMBACT.

■ REFERENCES

(1) Rehm, B. H. A. *Nat. Rev. Microbiol.* **2010**, *8*, 578−592.
(2) Bazaka, K.; Crawford, R. J.; Nazarenko, E. L.; Ivanova, E. P. In *Bacterial Adhesion*; Linke, D., Goldman, A., Eds.; Springer: New York, 2011; Chapter 13.
(3) Preiss, J. In *Bacteria in Nature: 3. Structure, Physiology, and Genetic Adaptability*; Leadbetter, E. R., Pointdexter, J. S., Eds.; Plenum Press: New York, 1989; Chapter 3.
(4) Dawes, E. A.; Ribbons, D. W. *Bacteriol. Rev.* **1964**, *28*, 126−149.
(5) Zevenhuizen, L. P. T. M.; Ebbink, A. G. *Antonie van Leeuwenhoek* **1974**, *40*, 103−120.
(6) Bender, H. *Eur. J. Appl. Microbiol. Biotechnol.* **1979**, *8*, 279−287.
(7) Voepel, K. C.; Buller, C. S. *J. Ind. Microbiol.* **1990**, *5*, 131−138.
(8) Sambou, T.; Dinadayala, P.; Stadthagen, G.; Barilone, N.; Bordat, Y.; Constant, P.; Levillain, F.; Neyrolles, O.; Gicquel, B.; Lemassu, A.; Daffé, M.; Jackson, M. *Mol. Microbiol.* **2008**, *70*, 762−774.
(9) Fishman, M. L.; Cescutti, P.; Fett, W. F.; Osman, S. F.; Hoagland, P. D.; Chau, H. K. *Carbohydr. Polym.* **1997**, *32*, 213−221.
(10) Hung, C. C.; Santschi, P. H.; Gillow, J. B. *Carbohydr. Polym.* **2005**, *61*, 141−147.
(11) Beech, I.; Hanjangsit, L.; Kalaji, M.; Neal, A. L.; Zinkevich, V. *Microbiology* **1999**, *145*, 1491−1497.
(12) Saravanan, P.; Jayachandran, S. *Lett. Appl. Microbiol.* **2008**, *46*, 1−6.
(13) Eboigbodin, K. E.; Biggs, C. A. *Biomacromolecules* **2008**, *9*, 686−695.
(14) Kansiz, M.; Heraud, P.; Wood, B.; Burden, F.; Beardall, J.; McNaughton, D. *Phytochemistry* **1999**, *52*, 407−417.
(15) Ngo Thi, N. A.; Naumann, D. *Anal. Bioanal. Chem.* **2007**, *387*, 1769−1777.
(16) Quilès, F.; Humbert, F.; Delille, A. *Spectrochim. Acta, Part A* **2010**, *75*, 610−616.
(17) Strathmann, M.; Wingender, J.; Flemming, H. C. *J. Microbiol. Methods* **2002**, *50*, 237−248.
(18) Yang, Y.; Sreenivasan, P. K.; Subramanyam, R.; Cummins, D. *Appl. Environ. Microbiol.* **2006**, *72*, 6734−6742.
(19) Nosyk, O.; ter Haseborg, E.; Metzger, U.; Frimmel, F. H. *J. Microbiol. Methods* **2008**, *75*, 449−456.
(20) Wu, J.; Deng, X.; Zhang, Y.; Wang, L.; Tian, B.; Xie, B. *Agric. Sci. China* **2009**, *8*, 1458−1465.
(21) Francius, G.; Lebeer, S.; Alsteens, D.; Wildling, L.; Gruber, H. J.; Hols, P.; De Keersmaecker, S.; Vanderleyden, J.; Dufrêne, Y. F. *ACS Nano* **2008**, *2*, 1921−1929.
(22) André, G.; Deghorain, M.; Bron, P. A.; van Swan, I. I.; Kleerebezem, M.; Hols, P.; Dufrêne, Y. F. *ACS Chem. Biol.* **2011**, *6*, 366−376.
(23) Dufrêne, Y. F. *Yeast* **2010**, *27*, 465−471.
(24) Radmacher, M. *Methods in Cell Biology*; Elsevier: New York, 2002; Chapter 4, Vol. *68*, p 67.
(25) Engel, A.; Müller, D. J. *Nat. Struct. Biol.* **2000**, *7*, 715−718.
(26) Francius, G.; Tesson, B.; Dague, E.; Martin-Jézéquel, V.; Dufrêne, Y. F. *Environ. Microbiol.* **2008**, *10*, 1344−1356.
(27) Francius, G.; Domenech, O.; Mingeot-Leclercq, M. P.; Dufrêne, Y. F. *J. Bacteriol.* **2008**, *190*, 7904−7909.
(28) Fischer, T. E.; Marszalek, P. E.; Fernandez, J. M. *Nat. Struct. Biol.* **2000**, *7*, 719−724.
(29) Hinterdorfer, P.; Dufrêne, Y. F. *Nat. Methods* **2006**, *3*, 347−355.
(30) Alsteens, D.; Garcia, M. C.; Lipke, P. N.; Dufrêne, Y. F. *Proc. Natl. Acad. Sci. U.S.A* **2010**, *107*, 20744−20749.
(31) Polyakov, P.; Soussen, C.; Duan, J.; Duval, J. F. L.; Brie, D.; Francius, G. *PLoS One* **2011**, *6*, e18887.
(32) Goldstein, I. J.; Hollerman, C. E.; Merrick, J. M. *Biochim. Biophys. Acta, Gen. Subj.* **1965**, *97*, 68−76.
(33) Goldstein, I. J.; Hayes, J. In *Advances in Carbohydrate Chemistry and Biochemistry*; Tipson, R. S., Horton, D., Eds.; Academic Press: New York, 1978; Vol. *35*, p 127.
(34) Griffiths, P. R.; de Haseth, J. A. *Fourier Transform Infrared Spectrometry*, 2nd ed.; Wiley-Interscience: Hoboken, NJ, 2007.
(35) Lévy, R.; Maaloum, M. *Nanotechnology* **2002**, *13*, 33−37.
(36) Vadillo-Rodríguez, V.; Busscher, H. J.; Norde, W.; De Vries, J.; Dijkstra, R. J. B.; Stokroos, I.; van der Mei, H. C. *Appl. Environ. Microbiol.* **2004**, *70*, 5441−5446.
(37) Francius, G.; Alsteens, D.; Dupres, V.; Lebeer, S.; De Keersmaecker, S.; Vanderleyden, J.; Gruber, H. J.; Dufrêne, Y. F. *Nat. Protoc.* **2009**, *4*, 939−946.
(38) Reiner, C. K.; Stroh, C. M.; Ebner, A.; Klampfl, C.; Gall, A. A.; Romanin, C.; Lyubchenko, Y. L.; Hinterdorfer, P.; Gruber, H. J. *Anal. Chim. Acta* **2003**, *479*, 59−75.
(39) Ebner, A.; Wildling, L.; Zhu, R.; Rankl, C.; Haselgrübler, P.; Gruber, H. J. *Top. Curr. Chem.* **2008**, *285*, 29−76.
(40) Hertz, H. *J. Reine Angew. Math.* **1881**, *92*, 156−171.
(41) Sneddon, I. N. *Int. J. Eng. Sci.* **1965**, *3*, 47−57.
(42) Arnoldi, M.; Fritz, M.; Bäuerlein, E.; Rodmacher, M.; Sackmann, E.; Boulbitch, A. *Phys. Rev. E* **2000**, *62*, 1034−1044.
(43) Ortiz, C.; Hadziioannou, G. *Macromolecules* **1999**, *32*, 780−787.
(44) Janshoff, A.; Neitzert, M.; Oberdörfer, Y.; Fuchs, H. *Angew. Chem., Int. Ed.* **2000**, *39*, 3212−3237.
(45) Abu-Lai, N. I.; Camesano, T. A. *J. Microsc.* **2003**, *212*, 217−238.

(46) Camesano, T. A.; Abu-Lai, N. I. *Biomacromolecules* **2002**, *3*, 661−667.
(47) Heinrisch, J. J.; Dupres, V.; Alsteens, D.; Dufrêne, Y. F. *Nat. Protoc.* **2010**, *5*, 670−677.
(48) Humbert, F.; Quilès, F.; Delille, A. In *Current Research Topics in Applied Microbiology and Microbial Biotechnology*; Mendez-Vilas, A., Ed.; World Scientific Publishing Co. Pte. Ltd.: 2009, p 268.
(49) Hong, K.; Sun, S.; Titan, W.; Chen, G. Q.; Huang, W. *Appl. Microbiol. Biotechnol.* **1999**, *51*, 523−526.
(50) Read, R. R.; Costerton, J. W. *Can. J. Microbiol.* **1987**, *33*, 1080−1090.
(51) Beech, I. B.; Gaylarde, C. C.; Smith, J. J.; Geesey, G. G. *Appl. Microbiol. Biotechnol.* **1991**, *35*, 65−71.
(52) Bahmed, K.; Quilès, F.; Bonaly, R.; Coulon, J. *Biomacromolecules* **2003**, *4*, 1763−1772.
(53) James, G. A.; Korber, D. R.; Caldwell, D. E.; Costerton, J. W. *J. Bacteriol.* **1995**, *177*, 907−915.
(54) Bentley, S. D.; Aanensen, D. M.; Mavroidi, A.; Saunders, D.; Rabbinowitsch, E.; Collins, M.; Donohoe, K.; Harris, D.; Murphy, L.; Samuel, G.; Skovsted, I. C.; Kaltoft, M. S.; Barrell, B.; Reeves, P. R.; Parkhill, J.; Spratt, B. G. *PLoS Genet.* **2006**, *2*, 0262−0269.
(55) Landersjö, C.; Yang, Z.; Huttunen, E.; Wildmalm, G. *Biomacromolecules* **2002**, *3*, 880−884.
(56) Meléndez, R.; Meléndez-Hevia, E.; Canela, E. I. *Biophys. J.* **1999**, *77*, 1237−1332.